International Journal of Humanoid Robotics Vol. 20, No. 4 (2023) 2350005 (23 pages) © World Scientific Publishing Company DOI: 10.1142/S0219843623500056



Design a Four-Bar Mechanism for Specific Upper Limb Muscle Strength Rehabilitation Using Genetic Algorithm

Joel Quarnstrom, Rahid Zaman and Yujiang Xiang* School of Mechanical and Aerospace Engineering Oklahoma State University, Stillwater, OK 74078 USA *yujiang.xiang@okstate.edu

> Received 31 July 2022 Revised 31 January 2023 Accepted 3 May 2023 Published 13 July 2023

In this study, a novel human-in-the-loop design method using a genetic algorithm (GA) is presented to design a low-cost and easy-to-use four-bar linkage medical device for upper limb muscle rehabilitation. The four-bar linkage can generate a variety of coupler point trajectories by using different link lengths. For this medical device, patients grab the coupler point handle and rotate the arm along the designed coupler point trajectory to exercise upper limb muscles. The design procedures include three basic steps: First, for a set of link lengths, a complete coupler point trajectory is generated from four-bar linkage kinematics; second, optimization-based motion prediction is utilized to predict arm motion (joint angle profiles) subjected to hand grasping and joint angle limit constraints; third, the predicted joint angles and given hand forces are imported into an OpenSim musculoskeletal arm model to calculate the muscle forces and activations by using the OpenSim static optimization. In the GA optimization formulation, the design variables are the four-bar link lengths. The objective function is to maximize a specific muscle's exertion for a complete arm rotation. Finally, different four-bar configurations are designed for different muscle strength exercises. The proposed human-in-the-loop design approach successfully integrates GA with linkage kinematics, arm motion prediction, and OpenSim static optimization for four-bar linkage design for upper limb muscle strength rehabilitation.

Keywords: Four-bar linkage; genetic algorithm; OpenSim; static optimization; motion prediction; muscle rehabilitation.

1. Introduction

According to the American Heart Association, over 7 million Americans suffered a stroke between 2013 and 2016. While many researchers investigate the science of stroke prevention, others develop methods for stroke rehabilitation. Recovery is common among many patients; however, due to neural plasticity about one-third of stroke victims carry the disability for a long time. Repetition of a specific task is an approach that therapists use to recover motor function after a stroke. Rehabilitation

^{*}Corresponding author.

is more effective when the patient is more involved. One method to make rehabilitation more effective for the patient is to use robotic devices which increase the number of repetitions that a therapist could impose.² According to Fortune Business Insights, the rehabilitation-robot market was approximately \$530 million in 2018 and projected to reach approximately \$2600 million by 2026.³ The yearly cost for stroke rehabilitation service utilization is around \$11,689 excluding the medication, which is not affordable for a lot of Americans.⁴ This cost can be reduced by developing low-cost rehabilitation devices.

There are two types of rehabilitation devices for the upper extremities: exoskeleton type and end-effector type. Exoskeletons are attached to the upper limb at multiple points. 5–14 These devices have a structure that resembles the human upper limb and can provide accurate force/torque to a specific joint as seen in Fig. 1(a). End-effector rehabilitation robots have only a single point of interaction. 15,16 They are ground-mounted and connected to the patient's hand or forearm as shown in Fig. 1(b). Ghannadi developed a parallelogram linkage-based end effector upper-extremity rehabilitation robot where model-in-loop is considered for the controller. The robot has two degrees of freedom (DOFs). Zhao et al. 17 developed a four-bar linkage-based single-DOF upper limb rehabilitation robot. The subject-specific target motion was regressed from a large amount of upper limb rehabilitation motions using a clustering-based machine learning technique. Then the linkage was synthesized to repeat the target motion for rehabilitation.

In addition, rehabilitation devices should have some characteristics like a human therapist. There are two practice modes for rehabilitation robots: passive mode and active mode.¹⁸ At the early stage of post-stroke therapy, a patient's arm is usually unresponsive. This stage requires control of the robotic arm's motion along a desired reference trajectory. This type of control is called passive control.¹⁹ RUPERT-IV²⁰ used a passive control strategy. In the active mode, the performance of the robot arises from subject contribution where the patient is performing actively during the movement and the robot assists only if needed.¹⁶ Zhang et al.¹⁶ developed an active control system for upper limb rehabilitation. The controller exerted minimum required forces to assist the subject, called assist-as-needed training during rehabilitation.

Numerous products on the market assist in rehabilitation of the upper arm affected by stroke; however, none of these devices target specific arm muscles. One of the

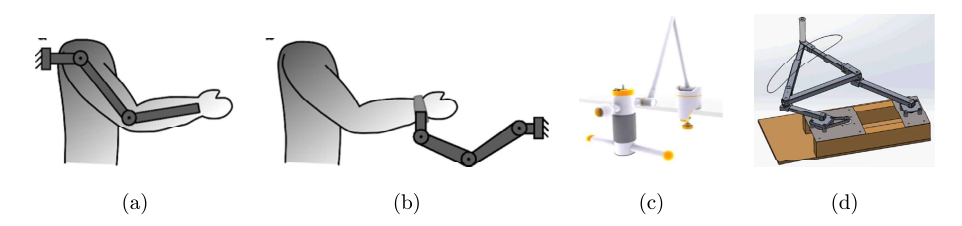


Fig. 1. (a) Exoskeleton type robot, (b) end-effector type rehabilitation robot, 21 (c) Saebo ReJoyce assistive robot, 22 and (d) four-bar linkage rehabilitation device.

available products in the market is the Saebo ReJoyce which is an end-effector rehabilitation robot. It has an armature that can move around freely. Users hold onto a grip, and they are directed to simulate the motion of certain tasks as shown in Fig. 1(c). These movements control computer simulations that provide the users with feedback. The goal of the device is to improve the user's strength and range of motion by simulating everyday tasks. While this solution is impressive, the motions it guides users to make require complicated control. The cost of the device is an issue as well. Figure 1(d) shows the designed prototype of the four-bar linkage rehabilitation device. Also, the users must be trained and supervised by qualified personnel while operating the device. Metcalf et al.²³ proposed a multi-domain dynamic model-based upper limb rehabilitation robot which had 2 DOFs and used position control instead of admittance or impendence control. Muscle targeted rehabilitation is a complex and challenging task but a very efficient way for patients' recovery. However, it requires subject-specific parameters for kinematic and dynamic modeling.²⁴ Also, the device/ robot should have the capability to change its geometry and control to optimize user's dynamics such as joint torques and muscle forces during human-robot interactions.²⁵ Gallagher et al.²⁶ proposed a method to control individual muscle force using an exoskeleton robot. However, it was a static task, and the subject did not change his or her posture during the task. The dynamics of the human and robot were neglected. Xiong and Manoonpong²⁷ proposed an adaptive controller for an elbow exoskeleton that provided resistance as needed for rehabilitation.

Current arm human-in-the-loop studies have produced intriguing control schemes for wearable robots used for rehabilitation or simple lifting assistance. Nasiri $et\ al.^{28}$ developed an adaptive control algorithm for exoskeleton lifting that simulated the arm muscle forces to determine the best exoskeleton torque. This control scheme is robust, but it requires a 7 DOF arm exoskeleton which will be bulky and expensive. Scotto di Luzio $et\ al.^{29}$ developed a controller for an end-effector rehabilitation robot that used the user's arm kinematics within the control algorithm. However, the arm muscle forces were not simulated. Ronsse $et\ al.^{30}$ controlled an elbow exoskeleton to adapt to arm oscillations using a simple damped pendulum model for the arm. This model also did not compute the arm muscle forces. There is a need for cheap arm rehabilitation devices that are controlled with human-in-the-loop algorithms that simulate the muscle forces. The cited rehabilitation devices and control methods are compared in Table 1.

In this study, we will design a portable, low-cost, and easy-to-use four-bar linkage end-effector rehabilitation robot for specific upper-limb muscle rehabilitation. A four-bar linkage morphology was selected so that the device would be simpler and cheaper while being able to achieve diverse hand trajectories. A four-bar linkage can be actuated with only one motor which reduces the cost. Having only one motor makes the device simpler and slimmer than devices with many motors. This reduces material cost as well as the cost of control electronics. It will be easy to use, because it will not require attaching multiple electrodes, straps, or components to the user's arm. Operation will only require setting a few parameters such as speed, resistance

Table 1. Comparison of upper limb rehabilitation devices.

${\rm Device/Method}$	Morphology	Active DOF per arm	Passive DOF per arm	Dynamic simulation	Simulated muscle forces	Reference
SAE-Exo	Elbow Exo.	0	4	No	No	Awad et al. ⁷
Shoulder Exoskeleton Using Parallel	Shoulder Exo.	က	2	No	No	Hunt et al. ⁹
Actuation and a Passive Slip In-						
terface						
Portable Elbow Exoskeleton for Three	Elbow Exo.	1	0	$N_{\rm o}$	No	Manna $et \ al.^{12}$
Stages of Rehabilitation						
Harmony	Upper Body Exo.	2		Yes	$N_{\rm o}$	Kim and $\operatorname{Deshpande}^5$
Parallel Cable-Driven Shoulder	Shoulder Exo.	1	2	$N_{\rm o}$	No	$Xu et al.^6$
Mechanism						
2 DOF Parallelogram Rehabilitation	End Effector	2	0	Yes	Yes	Ghannadi ¹⁵
Robot						
Immersive Rehabilitation Device for	End Effector	П	0	$^{ m No}$	No	Zhao $et al.^{17}$
Clustered Upper-Limb Motion						(
Cable-Driven Hybrid Shoulder	Shoulder Exo.	ਨ	0	$^{ m No}$	No	Niyetkaliyev $et al.^8$
Mechanism						
EULRR	Upper Body Exo.	7	0	Yes	$N_{\rm o}$	Zhang et al. 16
Spatial Gravity Balance Mechanism	Arm Exo.	0	4	$N_{\rm o}$	$N_{\rm o}$	Peng et al. 11
CAREX	Arm Exo.	4	0	$N_{\rm o}$	$N_{\rm o}$	Mao $et al.^{10}$
MyPAM	End Effector	2	0	Yes	No	Metcalf $et al.^{23}$
Control of Skeletal Muscle Forces via	End Effector and	variable	0	Yes	Yes	Gallagher $et \ al.^{26}$
Physical Human-Robot Interaction	Arm Exo.					
RUPERT	Arm Exo.	က	2	$N_{\rm o}$	No	Balasubramanian $et \ al.^{20}$
Optimize the Geometric and Dynamic	Arm Exo.	variable	0	Yes	$N_{\rm o}$	Blanchet $et al.^{25}$
Designs of Upper Limb						
Exoskeletons						
Adaptive Oscillator Exoskeleton	Elbow Exo.	П	0	Yes	No	Ronsse et al.
Control						
Bio-Cooperative End-Effector	End Effector	2	0	$_{ m No}$	$N_{\rm o}$	Scotto di Luzio $et al.^{29}$
Rehabilitation Robot						
Weight Compensation in Upper Lim	Arm Exo.	_	0	Yes	Yes	Nasiri et al. 28
Wearable Robots	Till Ti	-	c	V	Ž	V: 27
ALDE	EIDOW EXO.	1	O	168	ONT	Along and Manounpong

and duration. The lengths of the linkages of the device can be changed to affect the hand trajectory. Different configurations will be optimized to produce the best rehabilitation results for specific arm muscles. The simulation of the system's dynamics and the body's muscle forces is uncommon in rehabilitation device design. It is especially uncommon to be used in a 1 DOF device.

The basic idea is to move the arm through the coupler point trajectory (as a guide) to exercise muscle groups as shown in Fig. 1(d). The trajectory will be the path that the grip handle on the coupler linkage traces out. The coupler point on the four-bar linkage can generate a variety of trajectories with different shapes. These shapes have been studied and collected in the atlas in the literature 31 and used in many places in industry. There will be a grip at the coupler point that the users will hold on to with their hand. Additional wrapping is needed for safety. A motor will rotate the crank linkage slowly and cause the other linkages to move. This will cause the whole system to move, and the grip point will trace out a particular trajectory. In order to exercise certain muscle groups, individual trajectories will be designed to optimize the exertion on muscle groups. The benefit of using a four-bar linkage mechanism is that we can generate different end-effector motions by using only one motor, whereas other mechanisms need multiple motors. As a result, the cost and weight of the device are reduced significantly.

In addition, a novel GA-based human-in-the-loop design method is proposed to optimize the four-bar linkage medical device for upper limb muscle strength rehabilitation. This novel design method integrates GA with linkage kinematics, arm motion prediction, and OpenSim static optimization as shown in Fig. 2. The design variables are coupler and rocker link lengths which generate a coupler point (hand end-effector) trajectory through four-bar linkage kinematics. Then motion prediction is used to obtain arm joint angle profiles. These joint angles with hand reaction forces are further inputted into an OpenSim musculoskeletal shoulder model to calculate muscle forces and activations using static optimization. Finally, the GA cost function maximizes a user-specified muscle force and minimizes other major muscle forces over a complete arm rotation. This cost function is subject-specific and muscle-specific. The user's measured arm dimensions are used to scale the motion prediction model. GA optimization was selected because it is a non-gradient based global optimizer. The cost function of the optimization is so far removed from the input

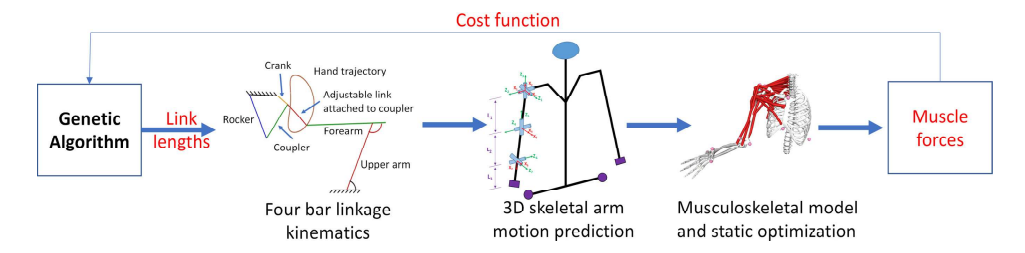


Fig. 2. GA-based human-in-the-loop design.

parameters that computing the gradients is impractical. Global optimization is preferred to local optimization in order to achieve the best results.

The contents are organized as follows: Section 2 presents the four-bar linkage kinematics to compute the coupler point trajectory. Section 3 describes the skeletal arm motion prediction to obtain joint angle profiles. Section 4 illustrates the OpenSim static optimization tool to calculate muscle forces and activations. Section 5 presents the general GA-based four-bar linkage optimization for upper limb muscle strength rehabilitation. Section 6 demonstrates the optimization results. The discussion and conclusions are given in Sec. 7.

2. Four-Bar Linkage Kinematics: Coupler Point Trajectory

The rehabilitation device consists of a four-bar linkage mechanism as shown in Fig. 3. The user holds onto a handle grip on p_5 . As the crank rotates, their hand is moved through a curvilinear trajectory. Link l_1 represents ground; link l_2 is the crank, which is driven by a motor; link l_4 is the rocker; and links l_3 , l_5 , and l_6 are coupler links which construct a rigid triangle. The link lengths of the linkage change for each design, and the position of the system is controlled by the crank angle θ . The linkage joint cartesian coordinates are defined as $p_i = \begin{bmatrix} x_i & y_i \end{bmatrix}^T$, where the origin is at point p_1 . At the end of the crank:

$$p_2 = l_2 \begin{bmatrix} \cos(\theta) \\ \sin(\theta) \end{bmatrix}. \tag{1}$$

The angles ϕ_1 and ϕ_2 are defined as

$$\phi_1 = \tan^{-1} \left(\frac{y_2}{l_1 - x_1} \right), \tag{2}$$

$$\phi_2 = \cos^{-1}\left(\frac{b^2 + l_4^2 - l_3^2}{2l_4 b}\right),\tag{3}$$

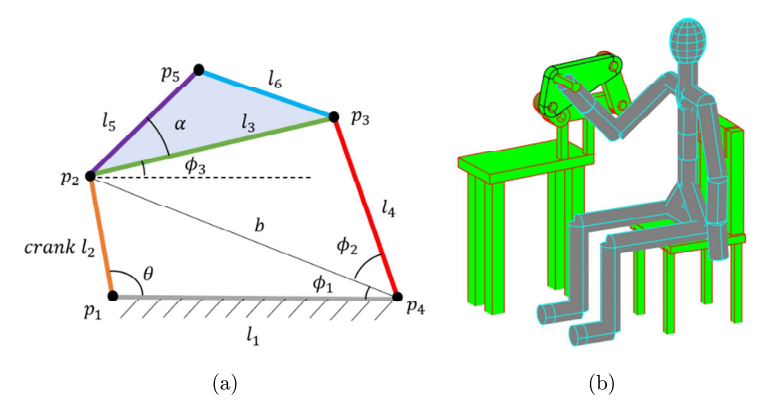


Fig. 3. (a) Four-bar linkage mechanism and (b) rehabilitation scenario.

where b is the variable length between p_2 and p_4 :

$$b = \sqrt{l_1^2 + l_2^2 - 2l_1 l_2 \cos(\theta)}. (4)$$

The point p_3 and angle ϕ_3 are

$$p_3 = \begin{bmatrix} l_1 \\ 0 \end{bmatrix} + l_4 \begin{bmatrix} -\cos(\phi_1 + \phi_2) \\ \sin(\phi_1 + \phi_2) \end{bmatrix}, \tag{5}$$

$$\phi_3 = \tan^{-1} \left(\frac{y_3 - y_2}{x_3 - x_2} \right). \tag{6}$$

This produces the coupler point position p_5 as

$$p_5 = p_2 + l_5 \begin{bmatrix} \cos(\phi_3 + \alpha) \\ \sin(\phi_3 + \alpha) \end{bmatrix}, \tag{7}$$

where α is defined by

$$\alpha = \cos^{-1}\left(\frac{l_3^2 + l_5^2 - l_6^2}{2l_3l_5}\right). \tag{8}$$

The rehabilitation context is pictured in Fig. 3(b). The four-bar linkage mechanism is mounted to a table, and the user is sitting on a chair next to it. The origin of the rehabilitation context is located directly below the user's spine on the floor. The chair, the human stick figure, and the table are defined as geometric objects that can be translated and rotated in the global coordinate frame. The kinematics of the linkages are calculated in a local reference frame that is defined based on the table's reference frame. This data is then transferred into the global coordinate system. The same process is done for the chair and the human model so that each object is represented in the global coordinate system.

3. Arm Motion Prediction

3.1. 3D skeletal arm model

The 3D skeletal arm model was created using the Denavit-Hartenberg (DH) method. Each body link is defined as a local coordinate system, and they are related to each other using 4×4 transformation matrices of the form:

$$\begin{array}{l}
i^{-1}T_{i} = \begin{bmatrix}
\cos(\theta_{i}) & -\sin(\theta_{i}) & 0 & 0 \\
\sin(\theta_{i}) & \cos(\theta_{i}) & 0 & 0 \\
0 & 0 & 1 & 0 \\
0 & 0 & 0 & 1
\end{bmatrix}
\begin{bmatrix}
1 & 0 & 0 & 0 \\
0 & 1 & 0 & 0 \\
0 & 0 & 1 & d_{i} \\
0 & 0 & 0 & 1
\end{bmatrix}
\begin{bmatrix}
1 & 0 & 0 & a_{i} \\
0 & 1 & 0 & 0 \\
0 & 0 & 1 & 0 \\
0 & 0 & 0 & 1
\end{bmatrix}$$

$$\times \begin{bmatrix}
1 & 0 & 0 & 0 \\
0 & \cos(\alpha_{i}) & -\sin(\alpha_{i}) & 0 \\
0 & \sin(\alpha_{i}) & \cos(\alpha_{i}) & 0 \\
0 & 0 & 0 & 1
\end{bmatrix}$$
(9)

$$i^{-1}T_i = \begin{bmatrix} \cos(\theta_i) & -\cos(\alpha_i)\sin(\theta_i) & \sin(\alpha_i)\sin(\theta_i) & a_i\cos(\theta_i) \\ \sin(\theta_i) & \cos(\alpha_i)\cos(\theta_i) & -\sin(\alpha_i)\cos(\theta_i) & a_i\sin(\theta_i) \\ 0 & \sin(\alpha_i) & \cos(\alpha_i) & d_i \\ 0 & 0 & 0 & 1 \end{bmatrix},$$
 (10)

where frame i-1 is the original reference frame, and frame i is the dependent reference frame. Each frame is defined by local coordinate axes x_i , y_i , and z_i . The variable θ_i is the angle around the z_{i-1} axis between x_{i-1} and x_i , d_i is the translation along the z_{i-1} axis between the two frames, a_i is the translation along the x_i axis between the two frames, and α_i is the rotation around x_i between z_{i-1} and z_i .

The matrix $^{i-1}T_i$ relates the coordinates of one link's frame (i) to the previous frame (i-1). These matrices are multiplied together to produce a matrix that relates the ith frame with the global reference frame:

$${}^{0}T_{i} = {}^{0}T_{1}{}^{1}T_{2}{}^{2}T_{3} \cdots {}^{i-1}T_{i}. \tag{11}$$

The right arm skeletal model has 7 DOFs: $\mathbf{q} = [q_1 \quad q_2 \quad \cdots \quad q_7]^T$ as in Fig. 4. The DH parameters are listed in Table 2, where the values for θ_i , d_i , a_i , and α_i are constant model parameters. The anthropometric data for the link lengths were found from the NASA Anthropometric Source Book Volume I.³³

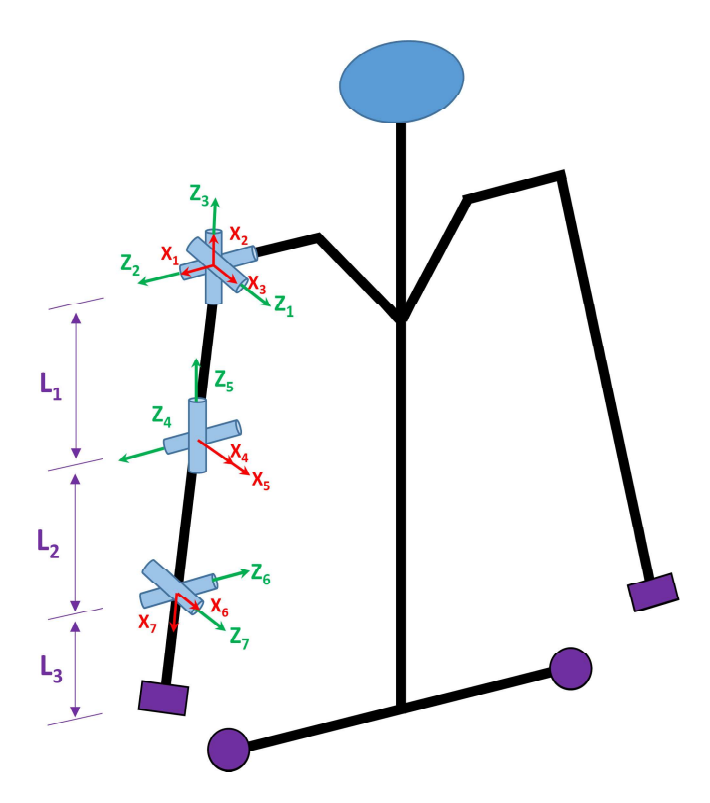


Fig. 4. 3D right arm skeletal model.

Joint names	θ	d	a	α
Shoulder adduction (q_1)	$-\pi/2$	0	0	$-\pi/2$
Shoulder flexion (q_2)	$-\pi/2$	0	0	$-\pi/2$
Shoulder rotation (q_3)	0	$-L_{\rm upper_arm}$	0	$\pi/2$
Elbow flexion (q_4)	0	0	0	$-\pi/2$
Elbow rotation (q_5)	0	$-L_{\text{fore_arm}}$	0	$-\pi/2$
Wrist flexion (q_6)	$\pi/2$	0	0	$\pi/2$
Wrist adduction (q_7)	0	0	$L_{ m hand}$	0

Table 2. Human upper body DH parameters.

3.2. Arm motion optimization formulation

The basis for the simulation starts with the generation of the four-bar linkage handle trajectory. Then, a nonlinear optimizer is used to solve for the arm joint angle profiles that cause the hand to be positioned in the same location as the handle. The kinematic simulation is performed in MATLAB, and the optimizer is MATLAB's fmincon function.

3.2.1. Design variables

The joint angle profiles are discretized by cubic B-splines,³⁴ so that the corresponding B-spline control points are treated as design variables, $\mathbf{x} = [c_1^{q_1} \dots c_7^{q_7}, \dots, c_1^{q_7} \dots c_7^{q_7}]^T$, where each joint angle profile is represented by 7 control points. Therefore, the total number of design variables is $7 \times 7 = 49$.

3.2.2. Objective function

The objective function was formulated to minimize the summation of the difference between the hand position and coupler (grip) point position, and the difference between the hand orientation and coupler handle orientation as

$$\operatorname{Min} J_{1} = \sum_{i=1}^{M_{\text{out}}} \|\boldsymbol{P}_{i}(\mathbf{x}) - \hat{\boldsymbol{P}}_{i}(\mathbf{L}, \boldsymbol{\theta}_{i}, t)\| + \sum_{i=1}^{M_{\text{out}}} \|\boldsymbol{H}_{i}(\mathbf{x}) - \hat{\boldsymbol{H}}_{i}(\mathbf{L}, \boldsymbol{\theta}_{i}, t)\|,$$
(12)

where P is the hand position calculated from arm model, \hat{P} is the four-bar linkage grip point position calculated from linkage kinematics, H is the hand orientation calculated from the arm model, \hat{H} is the four-bar grip handle orientation calculated from linkage kinematics, \mathbf{L} are four-bar link lengths, θ_i is the ith crank rotation angle, $M_{\text{out}} = T * \text{frequency}_1$ is the total number of hand position outputs for objective function J_1 , and T is the total time for one complete rotation.

3.2.3. Constraints

The joint angles are subject to joint angle limit constraints as

$$\mathbf{q}^{\mathrm{L}} < \mathbf{q}(\mathbf{x}) < \mathbf{q}^{\mathrm{U}},\tag{13}$$

where \mathbf{q}^{L} and \mathbf{q}^{U} are lower and upper joint angle limits obtained from the literature. ^{35–40}

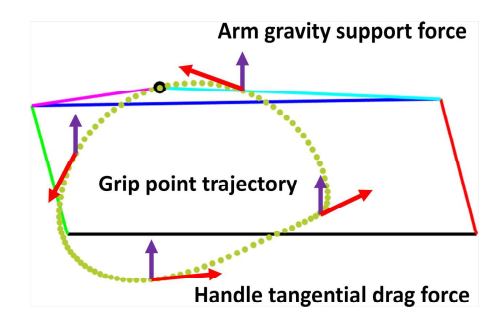


Fig. 5. Hand reaction forces

3.3. Hand reaction forces

The crank motor drives the four-bar coupler handle which interacts with the patient's hand. We assume there are two types of reaction forces applied on the hand at any time instant: one is the supporting force to balance the static weight of the arm pivoting about the shoulder, and the other is the handle dragging force along the tangential direction of the grip point trajectory as shown in Fig. 5.

In this study, a $30\,\mathrm{N}$ constant tangential drag force is used for four-bar linkage design. The upward supporting force is calculated at every time instant to balance the static arm moment equation at shoulder.

4. OpenSim Shoulder Model and Static Optimization

The musculoskeletal biomechanical analysis was performed using OpenSim.⁴¹ Open-Sim is a widely used open-sourced biomechanical software package for modeling, simulation, and analysis of neuromusculoskeletal systems. The static optimization tool of OpenSim is utilized to calculate the muscle forces for GA objective function.

4.1. An OpenSim musculoskeletal shoulder model

In this study, a modified Wu shoulder model⁴² as shown in Fig. 6 is employed, which has 5 segments and 12 DOFs. The model was actuated by 36 Hill-type muscle-tendon units. The model was developed and modified using OpenSim. The shoulder abduction—adduction and flexion—extension movements of the Wu shoulder model⁴² were generated by four complex joints: glenohumeral, scapulothoracic, sternoclavicular, and acromioclavicular joints. The 3D skeletal arm model cannot mimic these complex shoulder joints. Instead, we added 2 simplified DOFs to the shoulder joint of the Wu model to match the joint angles and rotational axes with the 3D skeletal model. One DOF models the simplified abduction-adduction movement and the other DOF models the simplified flexion—extension movement. We also added 10 new muscles to the shoulder and elbow joints to make the model suitable for an upper limb muscle rehabilitation task. Use of these muscles instead of an actuator for the elbow joint, will reduce the residual actuator value from the elbow during static

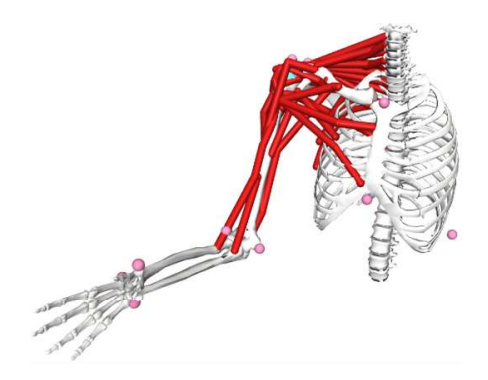


Fig. 6. Modified Wu shoulder model.

optimization. The additional muscles are one brachialis, one lateral triceps, one bicep longhead, one triceps longhead, one levator scapulae, three superior trapezius, one traverse trapezius and one inferior trapezius. The muscle properties were taken from Chadwick/ $et\ al.^{43}$ and van den Bogert $et\ al.^{44}$ The details of the Wu shoulder model can be found in Wu $et\ al.^{42}$

4.2. OpenSim static optimization

Static optimization in OpenSim is called to calculate muscle forces. First, the static optimization calculates the joint torques by plugging the predicted joint angles and given hand reaction forces into the equations of motion as follows. 45

$$\tau = \mathbf{M}(\mathbf{q})\ddot{\mathbf{q}} + \mathbf{C}(\mathbf{q}, \dot{\mathbf{q}}) + \mathbf{G}(\mathbf{q}) + \mathbf{E}(\mathbf{q}, \dot{\mathbf{q}}), \tag{14}$$

where τ is the muscular joint torque vector, \mathbf{q} is the joint angle vector, $\dot{\mathbf{q}}$ and $\ddot{\mathbf{q}}$ are joint velocity and acceleration vectors obtained from B-spline differentiations, $\mathbf{M}(\mathbf{q})$ is the system mass matrix, $\mathbf{C}(\mathbf{q}, \dot{\mathbf{q}})$ is the centrifugal and Coriolis force vector, $\mathbf{G}(\mathbf{q})$ is the gravitational loading vector, and $\mathbf{E}(\mathbf{q}, \dot{\mathbf{q}})$ is the external force vector.

At the second step, to calculate the muscle activations, the redundant system is solved at each time step by minimizing the muscle activation subjected to a muscle-torque equilibrium constraint. The joint torques obtained from the first step will be used in the constraint.

Find:
$$a_m$$

$$Min J_2 = \sum_{m=1}^{n} (a_m)^p$$

$$s.t.: \sum_{m=1}^{n} [a_m f(F_m^0, l_m, v_m)] r_{m,j} = \tau_j$$
(15)

where n is the number of muscles in the model, a_m is the activation level of muscle m at a discrete time step, F_m^0 is the maximum isometric force, l_m is muscle length, v_m is velocity, $f(F_m^0, l_m, v_m)$ is the muscle force-length-velocity surface, $r_{m,j}$ is its moment

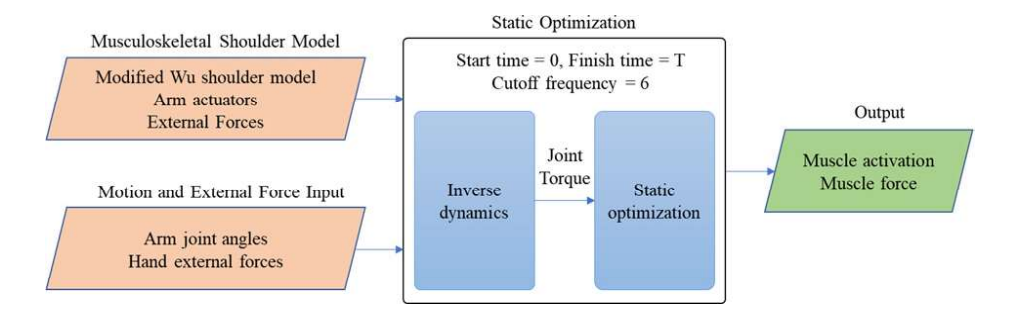


Fig. 7. Diagram of OpenSim static optimization API.

arm about the jth joint axis, τ_j is the joint torque acting about the jth joint axis, and p is a user-defined constant. Here, p is 2. After optimization, the muscle force can be calculated from muscle activation and contraction dynamics.^{46,47}

4.3. OpenSim application programming interface (API) setup

We used a MATLAB script (MATLAB 2022) to call the OpenSim API static optimization (OpenSim 4.3) to calculate muscle forces for each GA optimization iteration. The cut-off frequency was set to 6 Hz. The inputs of static optimization include the modified Wu shoulder model, joint angles, and hand reaction force profiles. The outputs are muscle force and activation profiles. The diagram of OpenSim API for static optimization is depicted in Fig. 7.

5. GA Design Optimization of the Four-bar Mechanism

5.1. GA optimization procedures

The GA in MATLAB is used to optimize the four-bar link lengths for upper limb muscle strength rehabilitation. In each iteration, for a set of link lengths, a complete coupler point trajectory is first generated from four-bar linkage kinematics. Then arm motion prediction is utilized to predict upper limb joint angles. After that, the predicted joint angles and given hand reaction forces are imported into the OpenSim musculoskeletal shoulder model to calculate the muscle forces by using the OpenSim static optimization. Next, GA is used to maximize a specific muscle exertion and minimize all other muscle exertions for a complete arm rotation. If the convergence condition is satisfied, the GA optimization stops, otherwise an inner loop is employed to restart the optimization. These procedures are depicted in Fig. 8.

5.2. GA optimization formulation

5.2.1. Design variables

In this study, the ground (l_1) and crank (l_2) link lengths are given and fixed. The design variables are the rocker link length $(l_r = l_4)$ and three coupler lengths $(l_{c1} = l_3, l_{c2} = l_5, l_{c3} = l_6)$. Therefore, $\mathbf{x} = \begin{bmatrix} l_3 & l_4 & l_5 & l_6 \end{bmatrix}^{\mathrm{T}}$.

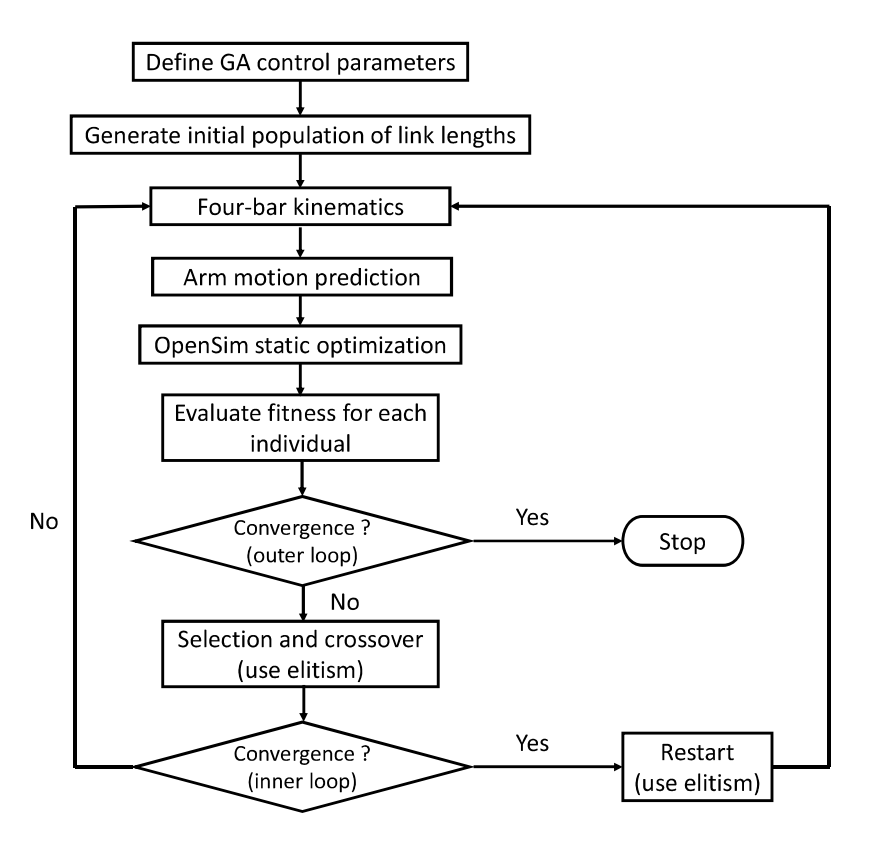


Fig. 8. GA-based four-bar design procedures.

5.2.2. Objective function

Two cases are studied in this work: one is to design a four-bar linkage to exercise the anterior deltoid muscle and the other is to design a four-bar linkage to exercise the lateral triceps muscle. Therefore, two different objective functions are proposed to practice two different muscles as follows:

$$\operatorname{Min} \quad J_{3} = -N\left(\sqrt{\sum_{i=1}^{N_{\text{out}}} f_{i_\text{DELTanterior}}^{2}}\right) + N\left(\sqrt{\sum_{i=1}^{N_{\text{out}}} f_{i_\text{DELTlateral}}^{2}}\right) + N\left(\sqrt{\sum_{i=1}^{N_{\text{out}}} f_{i_\text{DELTposterior}}^{2}}\right) + N\left(\sqrt{\sum_{i=1}^{N_{\text{out}}} f_{i_\text{BIClong}}^{2}}\right) + N\left(\sqrt{\sum_{i=1}^{N_{\text{out}}} f_{i_\text{TRIlong}}^{2}}\right) + N\left(\sqrt{\sum_{i=1}^{N_{\text{out}}} f_{i_\text{TRIlat}}^{2}}\right), \tag{16}$$

where $N_{\text{out}} = T * \text{frequency}_2$ is the total number of muscle force outputs for the objective function J_3 , $N(\cdot)$ is the normalization operator, and frequency₂ is the

muscle force data output frequency. The function J_3 maximizes the anterior deltoid muscle force while minimizing other major muscle forces.

$$\operatorname{Min} \quad J_{4} = N\left(\sqrt{\sum_{i=1}^{N_{\text{out}}} f_{i_\text{DELTanterior}}^{2}}\right) + N\left(\sqrt{\sum_{i=1}^{N_{\text{out}}} f_{i_\text{DELTlateral}}^{2}}\right) + N\left(\sqrt{\sum_{i=1}^{N_{\text{out}}} f_{i_\text{DELTlaterior}}^{2}}\right) + N\left(\sqrt{\sum_{i=1}^{N_{\text{out}}} f_{i_\text{BIClong}}^{2}}\right) + N\left(\sqrt{\sum_{i=1}^{N_{\text{out}}} f_{i_\text{TRIlat}}^{2}}\right) + N\left(\sqrt{\sum_{i=1}^{N_{\text{$$

where J_4 maximizes the lateral triceps muscle force while minimizing other major muscle forces. Note that the minimization is transformed into the maximization by multiplying a negative sign to the corresponding muscle forces in Eqs. (16) and (17).

5.2.3. Constraints

The link length limits are imposed as

$$\mathbf{x}^L \le \mathbf{x} \le \mathbf{x}^U,\tag{18}$$

where \mathbf{x}^{L} and \mathbf{x}^{U} are lower and upper bounds of link lengths. Note that the coupler (l_3) and rocker (l_4) link lengths' lower and upper bounds should be chosen to satisfy the four-bar linkage Grashof's law³¹ to generate a complete crank rotation. In addition, the coupler (l_6) link length limits depend on the other two coupler link lengths because they should build a coupler triangle.

6. Results

The following GA parameters are used in MATLAB: population size is 30 for each generation, the maximum generation is 100, the fitness function tolerance is 10^{-4} , and other parameters use the default values. The total time for a complete rotation is T=4 s. For arm motion prediction $M\text{out}=T\times \text{frequency}_1=4\times 3=12$ in Eq. (12), and for GA muscle force maximization $N\text{out}=T\times \text{frequency}_2=4\times 10=40$ in Eqs. (16) and (17).

6.1. Case 1: Design four-bar linkage to maximize anterior deltoid muscle force

For this case, the objective function Eq. (16) is used in the GA optimization formulation. It takes about 16.5 h for the GA to converge on a desktop computer with an Intel(R) Xeon(R) CPU E3-1270 v6 @3.80 GHz and 16 G RAM. The convergence history is depicted in Fig. 9. The optimal solution is $\mathbf{L} = [0.3500, 0.1150, 0.3500, 0.1203, 0.1106, 0.2407]^{\mathrm{T}}$ meters. Note that l_1 and l_2

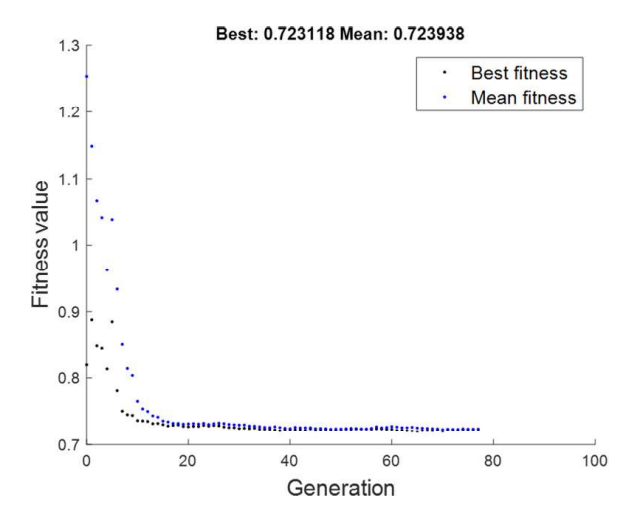


Fig. 9. GA convergence history for anterior deltoid muscle exercise (the upper dot line is the mean fitness, and the lower dot line is the best fitness).

are fixed and not optimized in this study. The optimal arm joint angle and torque profiles are shown in Fig. 10. The optimal muscle activations and forces are depicted in Fig. 11. The snapshots of the anterior deltoid rehabilitation arm exercise machine are shown in Fig. 12.

6.2. Case 2: Design four-bar linkage to maximize lateral triceps muscle force

For this case, the objective function Eq. (17) is used in the GA optimization formulation. It took about 12 h for the GA to converge on a desktop computer with the same configuration as the case 1. The convergence history is depicted in Fig. 13.

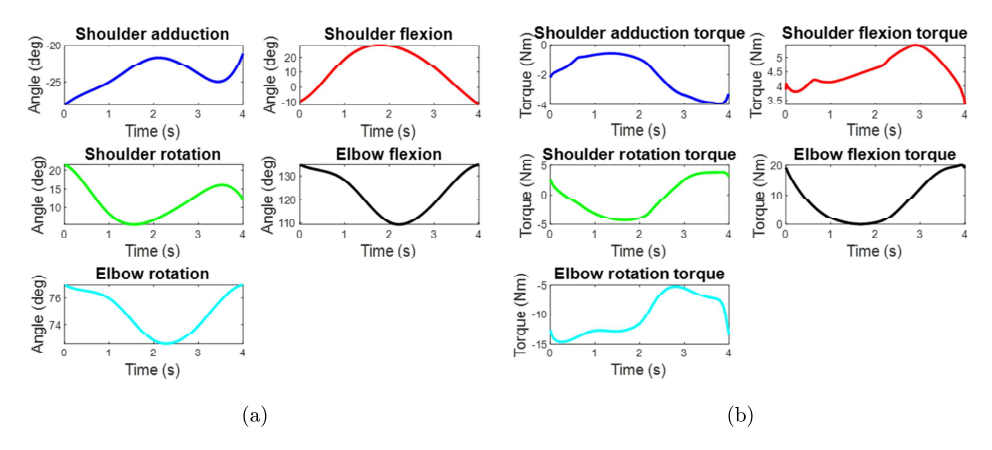


Fig. 10. Joint angle (a) and torque (b) profiles for anterior deltoid muscle exercise.

J. Quarnstrom, R. Zaman & Y. Xiang

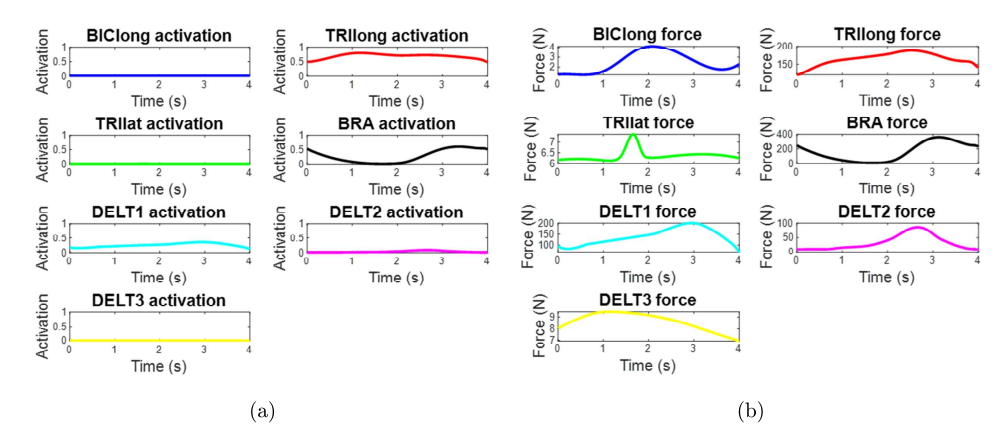


Fig. 11. Muscle activation (a) and force (b) profiles for anterior deltoid muscle exercise (BIClong is the biceps long head, TRIlong is the triceps long head, TRIlat is the triceps lateral, BRA is the brachialis, DELT1 is the anterior deltoid, DELT2 is the lateral deltoid, and DELT3 is the posterior deltoid).

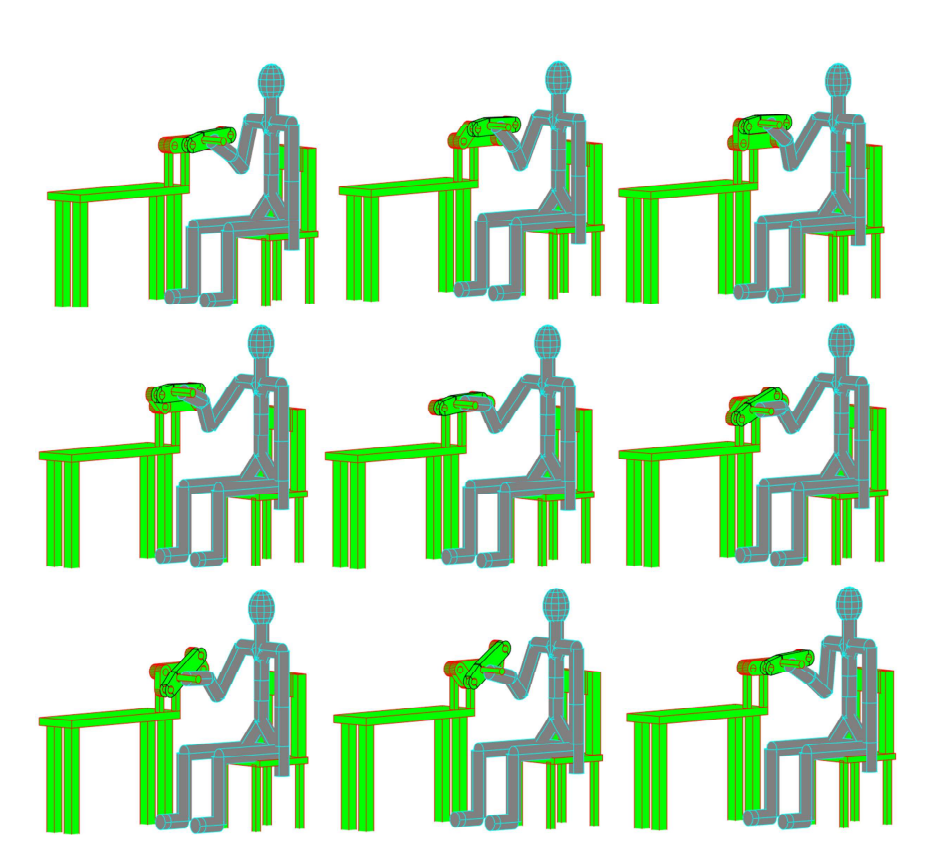


Fig. 12. Snapshots of arm rotation with optimal four-bar linkage design for anterior deltoid muscle rehabilitation.

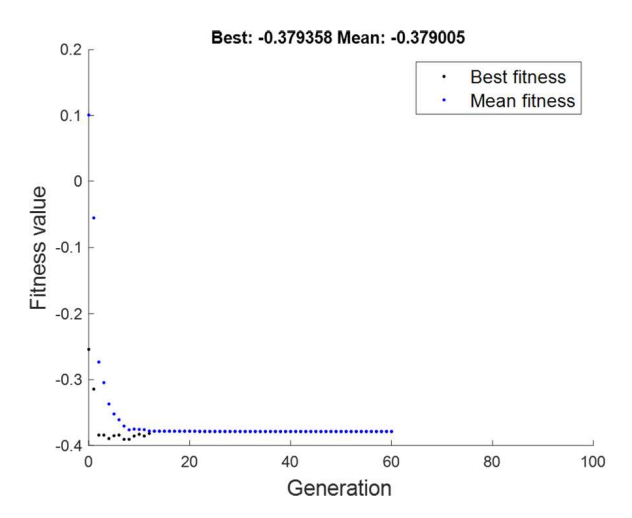


Fig. 13. GA convergence history for lateral triceps muscle exercise (the upper dot line is the mean fitness, and the lower dot line is the best fitness).

The optimal solution is $\mathbf{L} = [0.3500, 0.1150, 0.3664, 0.1675, 0.1933, 0.4139]^{\mathrm{T}}$ meters. Again, l_1 and l_2 are directly given and not optimized. The optimal arm joint angle and torque profiles are shown in Fig. 14. The optimal muscle activations and forces are depicted in Fig. 15. The snapshots of the lateral triceps rehabilitation arm exercise machine are shown in Fig. 16.

The skeleton model used in the simulation had dimensions based on the anthropometric data from the 50th percentile adult man.³³ The mounting position for the four-bar linkage on the simulated table was kept constant in all trials. The user's height and arm length as well as the four-bar mounting position and the relative position of the chair and table will affect the results of the simulation. These variables must be controlled in clinical applications to match the parameters from the

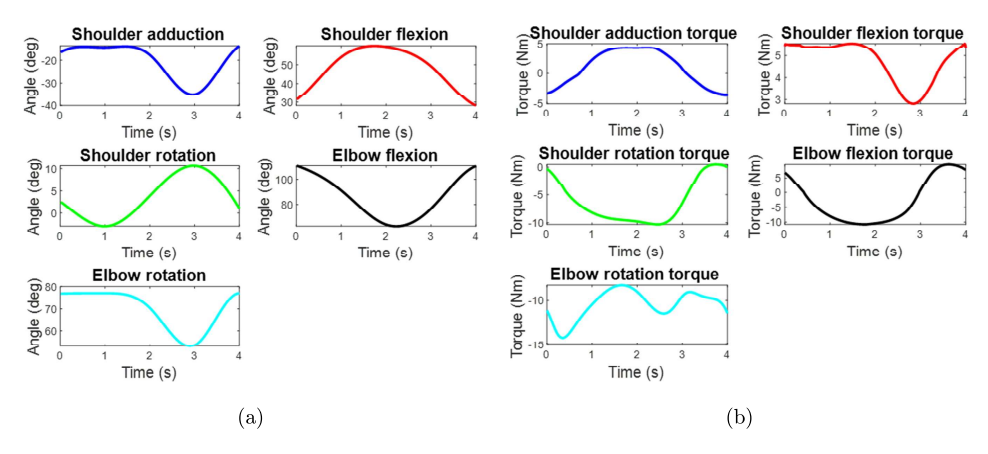


Fig. 14. Joint angle (a) and torque (b) profiles for lateral triceps muscle exercise.

J. Quarnstrom, R. Zaman & Y. Xiang

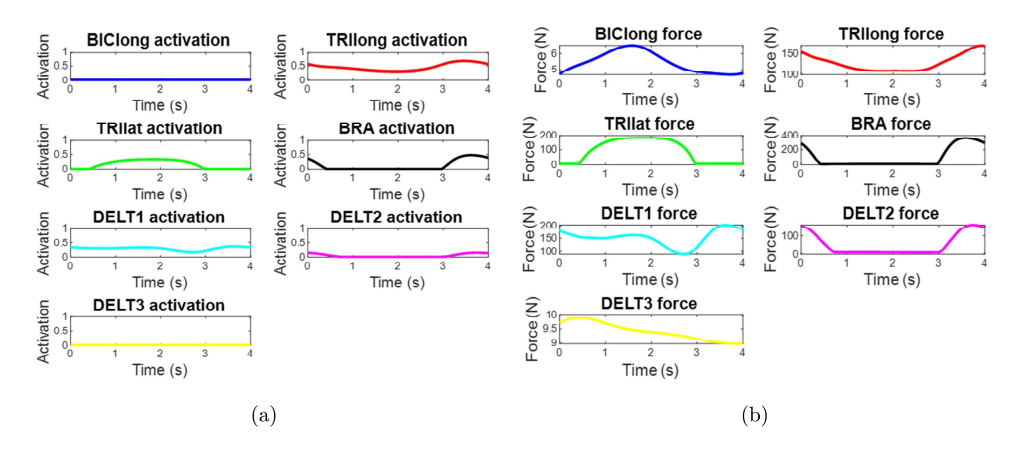


Fig. 15. Muscle activation (a) and force (b) profiles for lateral triceps muscle exercise.

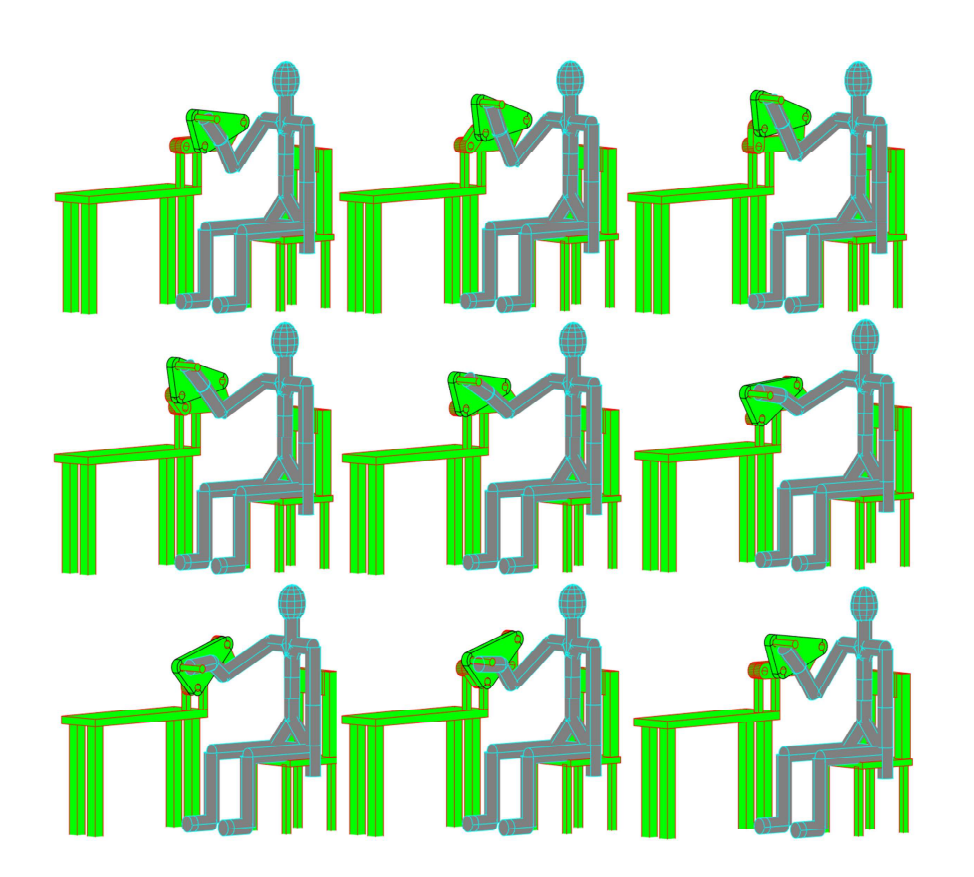


Fig. 16. Snapshots of arm rotation with optimal four-bar linkage design for lateral triceps muscle rehabilitation.

simulation. In this study, only one set of relative positions of the chair and table is used in the simulation. Variations of these dimensions will affect the simulation results. However, these dimensions are input parameters for the simulation. The simulation results can be easily updated based on different input parameters. The effect of varying these parameters on the rehabilitation quality could be studied in the future.

7. Discussion and Conclusions

In this study, we presented a new GA-based human-in-the-loop design method to optimize a four-bar linkage for upper limb muscle strength rehabilitation. The developed method efficiently integrated GA optimization with four-bar linkage kinematics, arm motion prediction, and OpenSim static optimization. The designed four-bar linkage medical device is subject-specific and muscle-specific. The proposed design method was demonstrated by optimizing two four-bar linkages for anterior deltoid and lateral triceps muscle exercises. The optimal four-bar link lengths were successfully obtained by solving a GA optimization problem. The GA convergence histories are shown in Figs. 9 and 13.

The hand and four-bar interaction forces were decomposed as an upward support force and a tangential drag force at every time instant. The arm motion prediction problem was solved by using the MATLAB fmincon solver to find the optimal joint angle profiles. Then the joint angle profiles and hand reaction forces were inputted into a 3D musculoskeletal shoulder model in OpenSim to calculate joint torques, muscle activations, and muscle forces. The GA successfully optimized arm motion and joint torque profiles (Figs. 10 and 14), and muscle activation and muscle force profiles (Figs. 11 and 15) for both the anterior deltoid muscle and the lateral triceps muscle strength exercises.

Since different cost functions were used for different muscle strength rehabilitation, the predicted muscle forces were different. For lateral triceps muscle rehabilitation, it is seen that the predicted peak value of the lateral triceps muscle force is around 200 N in Fig. 15(b). In contrast, the peak value of the lateral triceps muscle force for the anterior deltoid muscle rehabilitation in Fig. 11(b) is around 7 N which is much less than the lateral triceps muscle practice. This clearly demonstrates that the designed four-bar linkage for lateral triceps muscle practice does maximize the targeted muscle force. Another observation from Fig. 15(b) is that the lateral triceps muscle exercise also requires large deltoid muscle force which has a similar peak value as the anterior deltoid muscle exercise in Fig. 11(b). This can be explained by muscle coupling for generating the complete four-bar arm rotation, i.e., to exercise certain muscle, some major muscles must be used to complete the full arm rotation motion, and the shoulder deltoid muscle is such a major muscle for lateral triceps rehabilitation.

The snapshots of the arm rotations with optimal four-bar linkage designs for anterior deltoid and lateral triceps muscles were depicted in Figs. 12 and 16. The repeated cyclic motions were generated for muscle strength practice. It is seen that

the optimal four-bar linkage configurations for these two cases are different. Therefore, the generated grip point trajectories are also different.

In summary, it is promising to develop a low-cost and easy-to-use four-bar medical device for specific upper limb muscle rehabilitation. The proposed GA-based human-in-the-loop design approach is generic and can be applied to motions for other medical device designs as well. In the future, we will build a prototype to validate the simulation results.⁴⁸ In addition, we will also optimize the tangential hand reaction force in the GA. It will be interesting to allow negative drag force on the hand, which indicates a resistive force generated by a motor for upper limb muscle strength rehabilitation.

Acknowledgments

This work is partially supported by National Science Foundation (CBET 1849279 and 2014281), and Oklahoma State University Wentz research scholarship.

References

- E. J. Benjamin, P. Muntner, A. Alonso et al., Heart disease and stroke statistics-2019 update: A report from the American Heart Association, Circulation 139(10) (2019) 56-528.
- 2. S. Tahmid, J. Yang and J. M. Font-Llagunes, Review of models and robotic devices for stroke survivors' upper extremity rehabilitation, in *Proc. 2019 ASME International Design Engineering Technical Conference & Computers and Information in Engineering Conf.*, 18–21 August 2019, Anaheim, CA, USA.
- 3. Fortune Business Insights, Rehabilitation robots market size, share and industry analysis by type (Therapeutic robots, exoskeleton robots, assistive robots, others), by end user (rehabilitation centers, hospitals, others), regional forecast 2019–2026. (2019), https://www.fortunebusinessinsights.com/industry-reports/rehabilitation-robots-market-101013 (accessed on 1 June 2021).
- 4. K. M. Godwin, J. Wasserman and S. K. Ostwald, Cost associated with stroke: Outpatient rehabilitative services and medication, *Top. Stroke Rehabil.* **18** (2011) 676–684.
- 5. B. Kim and A. D. Deshpande, An upper-body rehabilitation exoskeleton Harmony with an anatomical shoulder mechanism: Design, modeling, control, and performance evaluation, *Int. J. Robotics Res.* **36**(4) (2017) 414–435.
- P. Xu, J. Li, S. Li, D. Xia, Z. Zeng, N. Yang and L. Xie, Design and evaluation of a parallel cable-driven shoulder mechanism with series springs, ASME J. Mech. Robotics 14(3) (2022) 031012.
- M. I. Awad, I. Hussain, S. Ghosh, Y. Zweiri and D. Gan, A double-layered elbow exoskeleton interface with 3-PRR planar parallel mechanism for axis self-alignment, ASME J. Mech. Robotics 13(1) (2021) 011016.
- 8. A. Niyetkaliyev, E. Sariyildiz and G. Alici, Kinematic modeling and analysis of a novel bio-inspired and cable-driven hybrid shoulder mechanism, *ASME J. Mech. Robotics* **13**(1) (2021) 011008.
- J. Hunt, H. Lee and P. Artemiadis, A novel shoulder exoskeleton robot using parallel actuation and a passive slip interface, ASME J. Mech. Robotics 9(1) (2017) 011002.

- Y. Mao, X. Jin and S. K. Agrawal, Real-time estimation of glenohumeral joint rotation center with cable-driven arm exoskeleton (CAREX)—A cable-based arm exoskeleton, ASME J. Mech. Robotics 6(1) (2014) 014502.
- Y. Peng, W. Bu and J. Chen, Design of the wearable spatial gravity balance mechanism, ASME J. Mech. Robotics 14(3) (2022) 031006.
- S. K. Manna and V. N. Dubey, A portable elbow exoskeleton for three stages of rehabilitation, ASME J. Mech. Robotics 11(6) (2019) 065002.
- X. Li, S. Liu, Y. Chang, S. Li, Y. Fan and H. Yu, A human joint torque estimation method for elbow exoskeleton control. *Int. J. Humanoid Robotics* 17(3) (2020) 1950039.
- G. Rigatos, M. Abbaszadeh, J. Pomares and P. Wira, A nonlinear optimal control approach for a lower-limb robotic exoskeleton, *Int. J. Humanoid Robotics* 17(5) (2020) 2050018.
- B. Ghannadi, Model-based control of upper extremity human-robot rehabilitation systems, PhD Thesis, University of Waterloo, Waterloo, Ontario, Canada (2017).
- L. Zhang, S. Guo and Q. Sun, Development and assist-as-needed control of an endeffector upper limb rehabilitation robot, Appl. Sci. 10(19) (2020) 6684.
- 17. P. Zhao, Y. Zhang, H. Guan, X. Deng and H. Chen, Design of a single-degree-of-freedom immersive rehabilitation device for clustered upper-limb motion, *ASME J. Mech. Robotics* **13**(3) (2021) 031006.
- T. Proietti, V. Crocher, A. Roby-Brami and N. Jarrasse, Upper-limb robotic exoskeletons for neurorehabilitation: A review on control strategies, *IEEE Rev. Biomed. Eng.* 9 (2016) 4–14
- E. P. Washabaugh, J. Guo, C. K. Chang, C. D. Remy and C. Krishnan, A portable passive rehabilitation robot for upper-extremity functional resistance training, *IEEE Trans. Biomed. Eng.* 66(2) (2018) 496–508.
- S. Balasubramanian, H. R. Wei, M. Perez, B. Shepard, E. Koeneman, J. Koeneman and J. He, RUPERT: An exoskeleton robot for assisting rehabilitation of arm functions, 2008 Virtual Rehabilitation, 25–27 August 2008, Vancouver, BC, Canada, pp. 163–167.
- A. Bertomeu-Motos, A. Blanco, F. J. Badesa, J. A. Barios, L. Zollo and N. Garcia-Aracil, Human arm joints reconstruction algorithm in rehabilitation therapies assisted by endeffector robotic devices, J. NeuroEng. Rehabil. 15(1) (2018) 1–11.
- L. U. Jensen, T. S. Winter, R. R. M. Jørgensen, D. M. Hellestrup and L. C. Jensen, Maintaining trust while fixated to a rehabilitative robot, in *The Eleventh ACM/IEEE Int.* Conf. Human Robot Interaction (IEEE Press, 2016), pp. 443–444.
- A. G. Metcalf, J. F. Gallagher, A. E. Jackson and M. C. Levesley, Multi-domain dynamic modelling of a low-cost upper limb rehabilitation robot, *Robotics* 10(4) (2021) 134.
- 24. M. Laitenberger, M. Raison, D. Périé and M. Begon, Refinement of the upper limb joint kinematics and dynamics using a subject-specific closed-loop forearm model, *Multibody Syst. Dyn.* **33**(4) (2015) 413–438.
- L. Blanchet, S. Achiche, Q. Docquier, P. Fisette and M. Raison, A procedure to optimize
 the geometric and dynamic designs of assistive upper limb exoskeletons, *Multibody Syst.*Dyn. 51(2) (2021) 221–245.
- W. Gallagher, M. Ding and J. Ueda, Relaxed individual control of skeletal muscle forces via physical human-robot interaction, Multibody Syst. Dyn. 30(1) (2013) 77–99.
- 27. X. Xiong and P. Manoonpong, Online adaptive resistance control of an arm exercise exoskeleton, in 23rd Int. Conf. Climbing and Walking Robots and the Support Technologies for Mobile Machines, 24–26 August 2020, Moscow, Russian Federation.
- 28. R. Nasiri, H. Aftabi and M. N. Ahmadabadi, Human-in-the-loop weight compensation in upper limb wearable robots towards total muscles' effort minimization, *IEEE Robotics Autom. Lett.* **7**(2) (2022) 3273–3278.

- F. Scotto di Luzio, D. Simonetti, F. Cordella, S. Miccinilli, S. Sterzi, F. Draicchio and L. Zollo, Bio-cooperative approach for the human-in-the-loop control of an end-effector rehabilitation robot, Front. Neurorobotics 12 (2018) 67.
- 30. R. Ronsse, N. Vitiello, T. Lenzi, J. Van Den Kieboom, M. C. Carrozza and A. J. Ijspeert, Adaptive oscillators with human-in-the-loop: Proof of concept for assistance and rehabilitation, in 2010 3rd IEEE RAS & EMBS Int. Conf. Biomedical Robotics and Biomechatronics, 26–29 September 2010, Tokyo, Japan, pp. 668–674.
- 31. R. L. Norton, Design of Machinery, 5th edn. (McGraw Hill, 2012).
- J. Denavit and R. S. Hartenberg, A kinematic notation for low pair mechanisms based on matrices, ASME J. Appl. Mech. 22 (1955) 215–221.
- E. Churchill, L. L. Laubach, J. T. Mcconville and I. Tebbetts, Anthropometric source book. Volume 1: Anthropometry for designers. NASA Reference Publication 1024, NASA Scientific and Technical Information Office (1978).
- Q. Wang, Y. Xiang, H. J. Kim, J. S. Arora and K. Abdel-Malek, Alternative formulations for optimization-based digital human motion prediction, in *Proc. 2005 Digital Human* Modeling for Design and Engineering Symp, 14–16 June 2005, Iowa City, IA. SAE Technical Paper 2005-01-2691.
- H. J. Chung, Y. Xiang, A. Mathai, S. Rahmatalla, J. Kim, T. Marler, S. Beck, J. Yang, J. S. Arora, K. Abdel-Malek and J. Obusek, A robust formulation for prediction of human running, in *Proc. 2007 Digital Human Modeling for Design and Engineering Symp.*, 12–14 June 2007, Seattle, WA. SAE Technical Paper 2007-01-2490.
- Y. Xiang, J. S. Arora, S. Rahmatalla and K. Abdel-Malek, Optimization-based dynamic human walking prediction: One step formulation, *Int. J. Numer. Methods Eng.* 79(6) (2009) 667–695.
- Y. Xiang, R. Zaman, R. Rakshit and J. Yang, Subject-specific strength percentile determination for two-dimensional symmetric lifting considering dynamic joint strength, Multibody Syst. Dyn. 46(1) (2019) 63-76.
- 38. Y. Xiang, J. Cruz, R. Zaman and J. Yang, Multi-objective optimization for twodimensional maximum weight lifting prediction considering dynamic strength, *Eng. Optim.* **53**(2) (2021) 206–220.
- R. Zaman, Y. Xiang, J. Cruz and J. Yang, Three-dimensional asymmetric maximum weight lifting prediction considering dynamic joint strength, J. Eng. Med. 235(4) (2021) 437–446.
- Y. Xiang and A. Arefeen, Two-dimensional team lifting prediction with floating-base box dynamics and grasping force coupling, Multibody Syst. Dyn. 50(2) (2020) 211–231.
- S. L. Delp, F. C. Anderson, A. S. Arnold, P. Loan, A. Habib, C. T. John, E. Guendelman and D. G. Thelen, OpenSim: Open-source software to create and analyze dynamic simulations of movement, *IEEE Trans. Biomed. Eng.* 54(11) (2007) 1940–1950.
- 42. W. Wu, P. V. Lee, A. L. Bryant, M. Galea and D. C. Ackland, Subject-specific musculoskeletal modeling in the evaluation of shoulder muscle and joint function, *J. Biomech.* **49**(15) (2016) 3626–3634.
- E. K. Chadwick, D. Blana, R. F. Kirsch and A. J. van den Bogert, Real-time simulation of three-dimensional shoulder girdle and arm dynamics, *IEEE Trans. Biomed. Eng.* 61(7) (2014) 1947–1956.
- A. J. van den Bogert, D. Blana and D. Heinrich, Implicit methods for efficient musculoskeletal simulation and optimal control, *Procedia IUTAM* 2 (2011) 297–316.
- A. Erdemir, S. McLean, W. Herzog and A. J. van den Bogert, Model-based estimation of muscle forces exerted during movements, Clin. Biomech. 22(2) (2007) 131–154.

- S. G. McLean, A. Su and A. J. van den Bogert, Development and validation of a 3-d model to predict knee joint loading during dynamic movement, J. Biomech. Eng. 125 (2004) 864–874.
- M. S. Shourijeh and J. McPhee, Forward dynamic optimization of human gait simulations: A global parameterization approach, ASME J. Comput. Nonlinear Dyn. 9 (2014) 031018.
- 48. M. A. Gull, S. Bai and T. Bak, A review on design of upper limb exoskeletons, *Robotics* 9(1) (2020) 16.



Joel Quarnstrom is a Mechanical and Aerospace Engineering PhD student studying Robotics and Controls at Oklahoma State University (OSU). He graduated with his B.S. in Mechanical Engineering with a second major in Physics in the Spring of 2022. He works in the Biodynamics Optimization and Motion Control Lab at OSU. In this lab, he has conducted research on a novel arm rehabilitation device, human-robot interaction biomechanics study, and a bio-inspired inchworm robot. He also collaborated

with an Electrical Engineering Lab at OSU on a home care robot intended to benefit the elderly.



Rahid Zaman is currently a postdoctoral research fellow in the Department of Mechanical and Aerospace Engineering at the University of Texas at Arlington. He received his B.S. in Mechanical Engineering from Military Institute of Science and Technology in 2013, M.S in Mechanical Engineering from University of Alaska Fairbanks in 2018, and Ph.D. in Mechanical Engineering from Oklahoma State University in 2022. His current research interests include human motion prediction, brain injury biomechanics, and robotics.



Yujiang (Mike) Xiang is currently an Associate Professor in the Department of Mechanical and Aerospace Engineering at Oklahoma State University (OSU). He received his B.S. and M.S. degrees in Automotive Engineering from Tsinghua University in 2001 and 2004, respectively, and Ph.D. degree from the University of Iowa in 2008. He directs the Biodynamics Optimization and Motion Control Lab in OSU. His current research interests include human robot interaction, musculoskeletal modeling, motion biomechanics, assistive robots, and exoskeletons.